Journal of Physics: Conference Series **684** (2016) 012006 doi:10.1088/1742-6596/684/1/012006

Use of shear waves for diagnosis and ablation monitoring of prostate cancer: a feasibility study

A Gomez[1], G Rus[2] and N Saffari[1]

[1] UCL Mechanical Engineering, University College London, Torrington Place, London WC1E 7JE, UK
[2] Department of Structural Mechanics, University of Granada, Politécnico de Fuentenueva, Granada 18071, Spain

E-mail: aj.gomez@ucl.ac.uk

Abstract. Prostate cancer remains as a major healthcare issue. Limitations in current diagnosis and treatment monitoring techniques imply that there is still a need for improvements. The efficacy of prostate cancer diagnosis is still low, generating under and over diagnoses. High intensity focused ultrasound ablation is an emerging treatment modality, which enables the non-invasive ablation of pathogenic tissue. Clinical trials are being carried out to evaluate its long-term efficacy as a focal treatment for prostate cancer. Successful treatment of prostate cancer using non-invasive modalities is critically dependent on accurate diagnostic means and is greatly benefited by a real-time monitoring system. While magnetic resonance imaging remains the gold standard for prostate imaging, its wider implementation for prostate cancer diagnosis remains prohibitively expensive. Conventional ultrasound is currently limited to guiding biopsy. Elastography techniques are emerging as a promising real-time imaging method, as cancer nodules are usually stiffer than adjacent healthy prostatic tissue. In this paper, a new transurethral approach is proposed, using shear waves for diagnosis and ablation monitoring of prostate cancer. A finite-difference time domain model is developed for studying the feasibility of the method, and an inverse problem technique based on genetic algorithms is proposed for reconstructing the location, size and stiffness parameters of the tumour. Preliminary results indicate that the use of shear waves for diagnosis and monitoring ablation of prostate cancer is feasible.

1. Background

Prostate Cancer (PCa) is the most common cancer in men in the UK. It is also the second cause of cancer death after lung cancer. It represents around 13% of all cases of cancer and accounts for 7% of all UK cancer deaths [1]. The incidence of PCa increases with age, affecting mainly men over 50 years of age [2]. The increase in longevity and awareness of the disease will lead to more men requesting screening, which will in turn increase the number of patients diagnosed with PCa in the future [3].

Prostate carcinoma is often suspected when the serum Prostate-Specific Antigen (PSA) is elevated or an abnormal digital rectal examination is noted. However, PSA screening leads to a substantial number of unnecessary biopsies in patients with no or indolent cancer, who do not need immediate treatment [4]. Histopathological evaluation of systematic biopsy cores is used to confirm or rule out cancer, and is normally carried out with conventional transrectal ultrasound as a guidance tool. Despite

the low specificity of PSA testing and the uncertainty after negative systematic biopsies, these techniques remain the standard for PCa diagnosis.

Current research is investigating whether modern imaging techniques can identify the site of the tumour. There are two main streams that are showing promising preliminary results: Magnetic Resonance Imaging (MRI) and Elastography techniques.

Multi-parametric MRI (mpMRI) combines T2-weighted imaging with functional sequences. It has become an important modality for tumour detection and staging [5,6], however, mpMRI performance varies depending on which combination of features is selected [7]. Additional limitations include cost, limited availability, contra-indication to MRI and contrast agents, and the fact that the very large majority of biopsies are ultrasound guided [8].

Prostate Elastography is an emerging imaging modality, which consists of the evaluation of prostate stiffness. Analogous to the cellular processes of wound repair, it is generally believed that normal tissue stroma responds in an effort to repair damage due to carcinoma cell invasion [9]. It has been concluded that the stromal reaction is also characterized by elevated collagen deposition [10]. Since increasing collagen deposition leads to an increase in the tumour rigidity, this suggests that quantitative stiffness estimations may prove to be an effective biomarker for assessing PCa grade and identification of more aggressive cancers [11].

Real-Time Elastography is available on some ultrasound systems for prostate imaging [12,13] and a few other techniques are currently being developed [13]. There are two main approaches commercially available:

- Quasi-Static (or Strain) Elastography (SE);
- Shear Wave Elastography (SWE).

SE of the prostate is based on the comparative analysis of tissue deformation before and after applying a slight static mechanical compression through the rectal wall. Stiffer tissue experiences less deformation than normal tissue. No quantitative elasticity analysis is available. Relative changes in the strain rate between zones work as a guide to suspect pathologic nodules existence [14]. This technique is commercially available for many clinical ultrasonic platforms [12]. SE limitations include:

- The lack of uniform compression over the entire gland;
- The intra and inter-operator dependency;
- Penetration issues in large prostate glands;
- Artefacts due to slippage of the compression plane.

SWE in PCa detection has been tested mainly by the Aixplorer ultrasound system transrectally (SuperSonic Imagine, Aix-en-Provence, France). In Transrectal-SWE (TR-SWE) by the Aixplorer system, acoustic radiation force produces a shear wave in the shape of a cone with a small inclination, which travels away from the pushing beam. An ultrafast scanner allows shear waves to be followed in real time in 2D, and echo tracking produces a displacement recording from which a small map of elasticity can be created [15]. Spatial resolution is worse than in SE imaging but the elastograms are quantitative.

Recent studies on PCa diagnosis using TR-SWE have shown very promising results [16–20]. The use of a 35 kPa threshold for Young's modulus to separate lesions from normal tissue in the Peripheral Zone may provide additional information for PCa detection and biopsy guidance, enabling a substantial reduction in the number of biopsies [16,17]. TR-SWE limitations include:

- The pressure artefacts induced by the transducer, as the end-fire design of the probe requires bending to image the mid prostate and apex;
- The slow frame rate, i.e. one image per second;
- The limited size of the region of interest (concretely only half of the prostate is covered);
- The delay to stabilize the signals at each acquisition plane;
- The signal attenuation in large prostates making the evaluation of the anterior Transitional Zone difficult or impossible [8].

The aim of this study is to evaluate the feasibility of using a Transurethral-SWE (TU-SWE) approach for diagnosis and High Intensity Focused Ultrasound (HIFU) ablation monitoring of PCa. This approach encompasses both the transmission and the detection of the shear wave propagation. Shear waves are propagated into the prostate as the result of applying torsional stress on the urethra wall at a localized point. If stiff lesions are presented in the prostate, the wavefront would suffer reflections due to the change in acoustic impedance. This reflection would travel back to the urethra where it could be detected (Figure 1). The parameters which define the tumour (location, size and stiffness) can be reconstructed from those recovered signals.

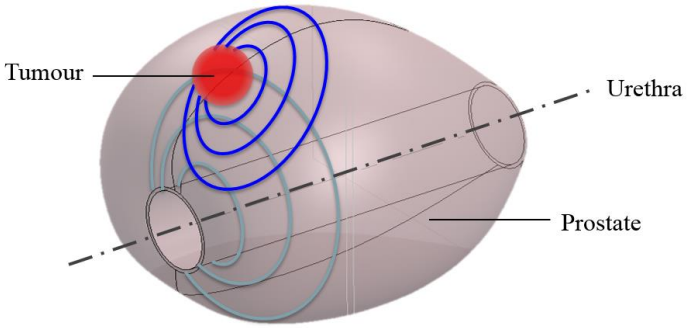

Figure 1. Conceptual idealization of the TU-SWE approach for diagnosis and ablation monitoring of PCa

The capability of transmitting shear waves into the prostate by mechanical contact through the urethra wall was evaluated in phantoms and *in vivo* canine experiments, by using a mechanical transurethral actuator as excitation force and MRI Elastography for measuring the displacement [21,22].

HIFU ablation is a promising focused technique for treating PCa, currently under clinical evaluation in several clinics around the world. As with other focused therapies it requires that the treated region be controlled and monitored to avoid damage of the surrounding healthy tissue. The TU-SWE approach allows the monitoring of HIFU ablation from the rectum, since the ultrasonic beam itself generates an alteration of the stiffness at the focal point and surroundings as the temperature increases during the surgery [23,24].

Inherent advantages of the TU-SWE approach proposed are listed below:

- The Transitional Zone and the Central Zone of the prostate (Figure 2) remain less accessible when using techniques that operate from the rectal passage. The urethral approach makes these zones more reachable. The Central Zone presents the lowest rate of PCa, but these cancers tend to be more aggressive and more likely to invade the seminal vesicles [25]. The TR-SWE studies are limited to the Peripheral Zone since this approach makes it difficult to reach the anterior zones of the prostate [16]. On the other hand, the reduction of tissue path is directly connected to the diminution of attenuation, which is a crucial matter in shear wave propagation.
- The possibility of using higher frequencies (above 500 Hz) than other techniques. This fact is related to the reduction in attenuation, which allows a slight increase of the excitation frequency, and therefore the spatial resolution, thus improving the imaging quality and the capacity of detecting smaller cancer nodules.
- Current techniques present difficulties in scanning the whole gland in a short time. TR-SWE covers only half of the prostate for every 2D scan. Although SE can cover complete 2D sections of the prostate, it presents problems covering the whole gland due to the challenge of keeping the pressure constant at every scan. Due to the geometrical configuration of the proposed TU-SWE approach, the whole gland volume may be covered simultaneously, permitting the opportunity of 3D real-time monitoring technique.

- In comparison with techniques that use acoustic radiation force, lower levels of energy are expected, and therefore lower ultrasound thermal and mechanical indices.
- The use of the urethra as a channel for diagnosis keeps the rectal passage free for transrectal therapies such as HIFU ablation.

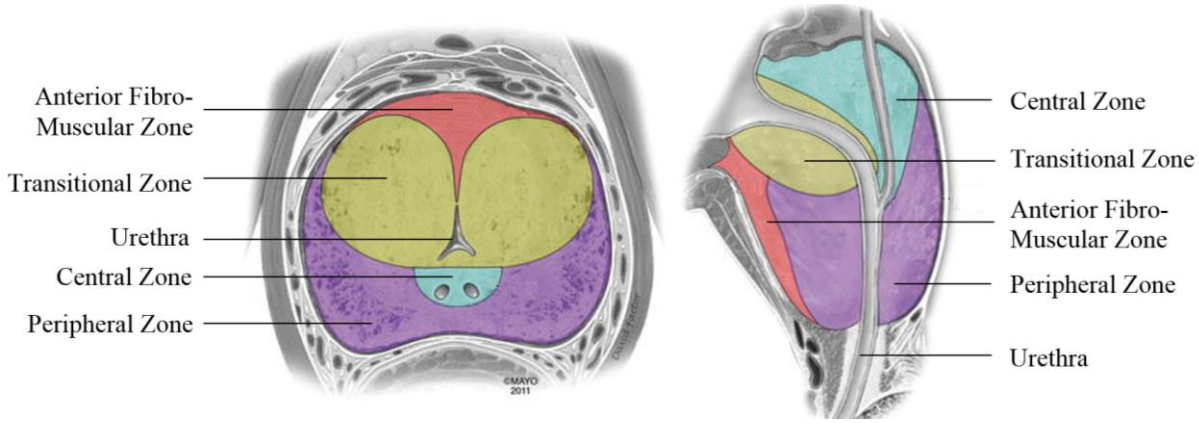

Figure 2. McNeal's anatomic division of the prostate. Source: Mayo Foundation for Medical Education and Research [26].

In this paper, a prostate-like medium is modelled using the Finite-Difference Time Domain (FDTD) method to investigate the PCa detection sensitivity of the proposed approach. An Inverse Problem (IP) based on genetic algorithms was developed for reconstructing the parameters that locate and size prostate nodules. Finally, the results from the reconstruction were analyzed to demonstrate the feasibility of the TU-SWE approach for diagnosis of PCa.

2. Methodology

2.1. Finite-Difference Time Domain model

A FDTD method is developed for simulating the propagation of shear waves into the prostate from the urethra. The FDTD method has been extensively used for modelling different physics phenomena in solid materials, mainly in electromagnetism and geophysics, but also for wave propagation in elastic and viscoelastic media [27,28]. Two aims are pursued with this model. One is to study, in a simple way, the feasibility of reflection detection in the PCa application. The other is to feed the reconstruction method, obtaining potential solutions which are tested iteratively in the inverse procedure.

The mechanical response of soft tissues is well known for a viscoelastic behaviour. In this study, an elastic model has been considered sufficient due to the absence of consensus about mechanical models and values for viscous parameters of prostatic tissue.

A cylindrical coordinate system is selected for establishing the discretization grid. The simplified prostate-like model is defined geometrically as a hollow cylinder, where the inner passage corresponds to the urethra (Figure 3).

Although the equations of motion can be formulated in several ways, a velocity-stress formulation was chosen [29], where time distributions of velocity and stress at spatial points are propagated along a regular grid to which material properties and the excitation source are assigned. Generally, a system of nine first-order hyperbolic equations are needed. Shear waves are generated by the application of torsional forces in the urethra wall in an axisymmetric configuration, and thus, together with the simplification of using a two dimensional approach, reduces the complexity to only one velocity component v_θ. The plane selected (in red colour Figure 3) contains the axis. The remaining three first-order hyperbolic equations (1-3) are expressed in terms of the stress tensor σ and velocity v_θ for an elastic medium. As a result of the simplification, the circular tumour in the plane becomes a torus in 3D.

Although this geometrical distribution is not representative of PCa, it can be considered acceptable for a proof of principle approach.

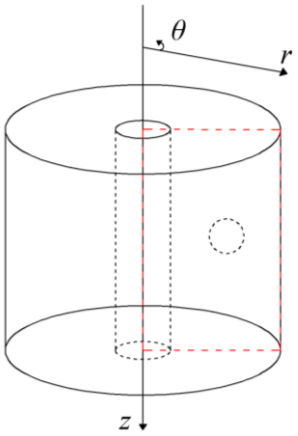

Figure 3. Simplified geometry for the model. 2D section of study in red. Spherical tumour.

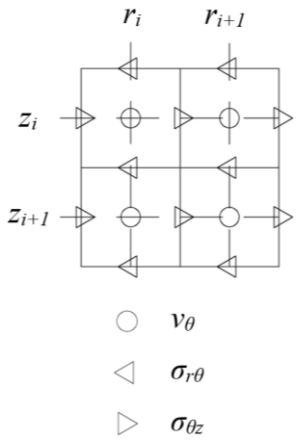

Figure 4. Diagram of the staggered grid discretization with positions of the variables.

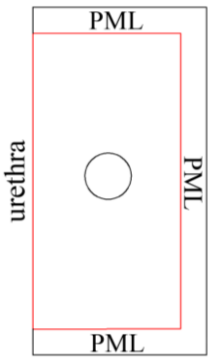

Figure 5. Spatial distribution of the model. Main domain in red. PML surrounding it. Urethra at left side.

$$\rho \dot{v}_\theta = \frac{\mathrm{d}\sigma_{r\theta}}{\mathrm{d}r} + \frac{\mathrm{d}\sigma_{\theta z}}{\mathrm{d}z} + \frac{2}{r}\sigma_{r\theta} \tag{1}$$

$$\dot{\sigma}_{r\theta} = \mu\left(\frac{\mathrm{d}v_\theta}{\mathrm{d}r} - \frac{v_\theta}{r}\right) \tag{2}$$

$$\dot{\sigma}_{\theta z} = \mu\frac{\mathrm{d}v_\theta}{\mathrm{d}z} \tag{3}$$

The mass density ρ and the shear modulus μ vary depending on whether they belong to the background tissue or to the cancer nodule. Spatial discretization is achieved with the staggered grid illustrated in Figure 4, i.e., the velocity component is specified at grid positions that are offset by a half-step from the corresponding stress components. Time is uniformly sampled via $t=n\Delta t$ for an integer n and interval Δt. Similarly, space is uniformly sampled, with $r=i\Delta r$ and $z=j\Delta z$ for integers i, j.

To propagate spatial quantities in time, the classical time-staggering approach is often used to estimate stress and velocity in alternating time intervals. In this case, an alternative method has been chosen, computing both magnitudes at each time interval starting from an initial situation at rest [27].

All temporal and spatial derivatives in equations (1), (2) and (3) are discretized using the following differencing schemes:

$$\dot{g}\big|_{r_i,t_{n+1}} = \frac{\mathrm{d}g}{\mathrm{d}t}\bigg|_{r_i,t_{n+1}} = \frac{g^{n+1}(i) - g^n(i)}{\Delta t} + \mathrm{O}(\Delta t) \tag{4}$$

$$g_{,r}\big|_{r_i,t_n} = \frac{\mathrm{d}g}{\mathrm{d}x}\bigg|_{r_i,t_n} = \frac{g^n\left(i+\frac{1}{2}\right) - g^n\left(i-\frac{1}{2}\right)}{\Delta r} + \mathrm{O}(\Delta r^2) \tag{5}$$

To reduce numerical dispersion we choose a minimum rate of 20 spatial intervals per wavelength λ as described in equation (6) although lower rates can be found in the literature. The temporal interval satisfies the stability condition (7) obtained from the Von Neumann condition [30].

$$20\max(\Delta r, \Delta z) < \lambda_{\min} \tag{6}$$

$$\max(c_s)\Delta t < \left(\frac{1}{\Delta r^2} + \frac{1}{\Delta z^2} \right)^{-1/2} \tag{7}$$

The rotational excitation is introduced in the model by setting v_θ at the corresponding points in the grid within the urethra wall where the torsion is applied.

In order to avoid reflections at outer boundaries of the domain, a Perfectly Matched Layer (PML) absorber is incorporated surrounding the main domain, excepting the urethra wall (Figure 5), using an adaptation for cylindrical coordinates [31].

2.2. Inverse Problem based on Genetic Algorithms

A way to solve an IP is to use the forward problem to find a solution for a set of parameters that minimizes the difference between the predicted and the actual measurements by using an optimization algorithm [32]. For this study a genetic algorithm is proposed for the optimization. The tumour parameters are contained in a vector named p_c. These parameters are: the radial r_c and depth z_c coordinates of the centroid of the nodule, the diameter $ø_c$ and the stiffness μ_c of the tumour.

Considering that this work is at a preliminary stage, experimental results are not yet available. To study the suitability of the proposed reconstruction method, pseudo-experimental signals u_{exp} were generated by adding white noise to signals simulated using the FDTD model.

The optimization algorithm will minimize the discrepancy between u_{exp} and the numerically predicted trial response $u(p_c)$, which is a function of the four-dimensional hyperspace formed by the four tumour parameters. To quantify the discrepancy, a cost functional f is designed, defined as the squared Euclidean distance between both measurements (8) [33].

$$f(p_c) = \left\| u_{\exp} - u(p_c) \right\|_2^2 \tag{8}$$

3. Results

3.1. Numerical model results

A numerical simulation was carried out by using the FDTD method described in Section 2.1. Figure 6 depicts the selected set-up. Note that the problem has been simplified after taking advantage of the axisymmetry of the cylindrical system shown in Figure 3.

The values corresponding to the labeled variables in Figure 6 are listed in Table 1. Those values and proportions are in agreement with those that can be found in a real human prostate. A rounded shape is selected to represent the cancerous nodule using an arbitrary, but realistic, value of 4 mm of diameter. The excitation source is located on the urethra wall, at centered depth. A set of 18 receivers is uniformly distributed for recording the signals coming from the interior of the domain.

Table 2 shows the values for mechanical parameters of both healthy and cancerous prostate, as well as the settings of the excitation source, which is implemented as a Gaussian modulated wave with central frequency of 1 kHz. Shear modulus values have been chosen in agreement with those found in the literature [16,17].

Table 3 lists the parameters for the numerical discretization. In order to guarantee an adequate visual resolution of the simulation, the discrete spatial values go beyond the stability condition described by equation (6), resulting in a total of 731,600 elements. The Von Neumann condition defined by equation (7) is applied to calculate the temporal discretization interval.

The simulation was performed using MATLAB® in conjunction with the Parallel Computing Toolbox™ (Release 2014b, MathWorks, Natick, United States). Run times lasted 406 seconds on a quad-core 3.60 GHz, 16 GB RAM, desktop computer.

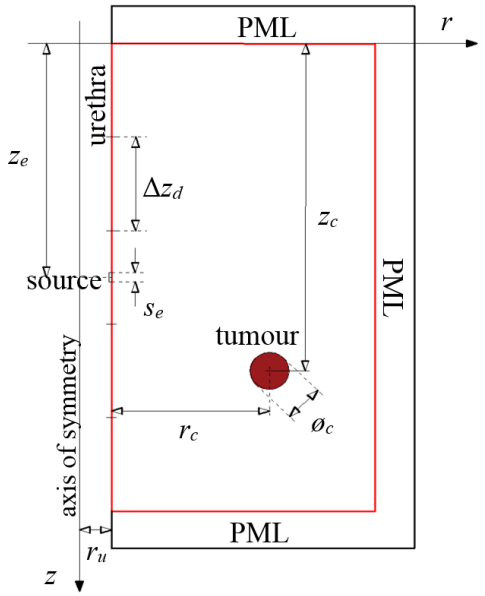

Figure 6. Schematic of set-up for numerical simulation. Tumour in red. Dimensions are described in Table 1.

Table 1. Dimension values for set-up of the numerical simulation.

Variable	Description	Value (mm)
r_d	Radial dimension of the domain	23.50
z_d	Depth dimension of the domain	50.00
r_u	Radius of urethra	3.25
z_e	Depth coordinate of excitation source	25.00
s_e	Thickness of excitation source	1.00
r_c	Radial coordinate of the tumour	14.00
z_c	Depth coordinate of the tumour	35.00
$\varnothing_c$	Diameter of the tumour	4.00
Δz_r	Distance between receivers	2.38

Table 2. Values for mechanical parameters and excitation [16,17]

Variable	Description	Value
ρ_h	Density of healthy tissue	1000 kg m^{-3}
μ_h	Shear modulus of healthy tissue	6.00 kPa
ρ_c	Density of cancerous tissue	1000 kg m^{-3}
μ_c	Shear modulus of cancerous tissue	18.00 kPa
f_c	Central frequency	1.00 kHz
t_T	Total time of simulation	25 ms
a	Source amplitude	10.00 µm

Table 3. Discretization parameters for FDTD simulation

Variable	Description	Value
Δr	Radial dimension interval	50 µm
Δz	Depth dimension interval	50 µm
Δt	Time interval	8.33 µs
n_{PML}	Number of PML elements	120

Figure 7 shows four snapshots of the simulated transient propagation of shear waves in a prostate-like medium containing a cancerous lesion, at different times when the wavefront hits and propagates across the tumour. It can be clearly seen how the reflections are generated traveling back to the urethra wall, as well as the ongoing wavefront accelerates while propagating across the tumour due to the higher velocity of the shear waves, 4.24 ms^{-1} against 2.45 ms^{-1} in the healthy tissue. A second reflection coming from the bottom of the tumour can be also visualized. The recordings at the receivers during the simulation are displayed in Figure 8.

3.2. Reconstruction IP-AG method results

In order to obtain a proof of feasibility for the IP-GA method, an example reconstruction is shown in this section.

As mentioned in Section 2.2, a simulated signal generated by the FDTD model with added white noise was used as an experimental signal to be reconstructed by the IP-GA method. The amplitude of the white noise signal corresponded to 10% of the root-mean-square of the simulated signal amplitude. The set-up for the pseudo-experimental signal was the same as the one in Section 2.1 (see Figure 6 and Tables 1 and 2). Table 4 shows the values of the parametrization. In this case, a coarser grid was chosen in order to speed up the iteration process and reduce the computational time. The pseudo-experimental

signal was detected by a receiver located 12.5 mm below the source on the urethra wall. The reconstruction algorithm was implemented using MATLAB® and the Parallel Computing Toolbox™ (Release 2014b, MathWorks, Natick, United States), lasting for 1204 seconds on the computer mentioned above. A population of 10 candidate solutions was selected, to be updated during 13 generations.

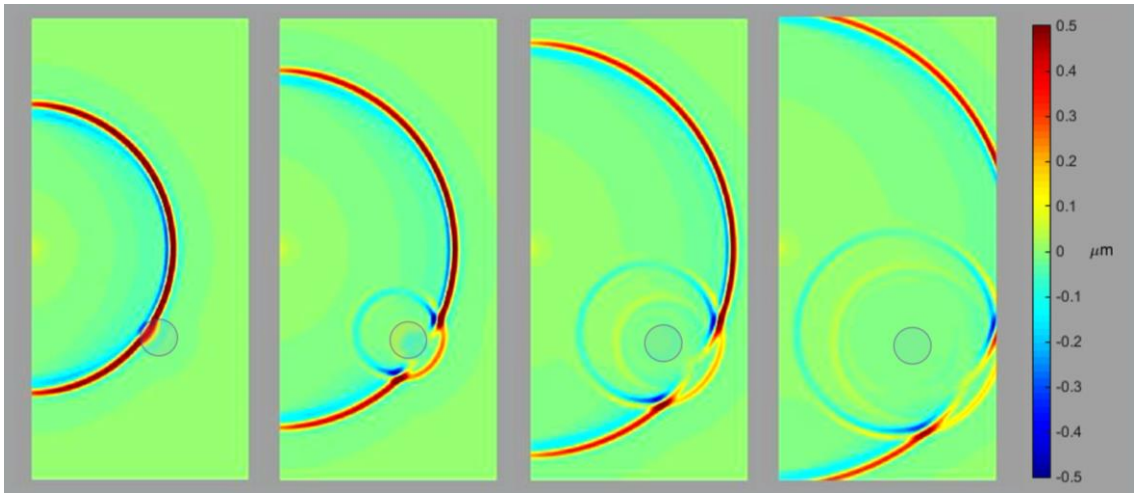

Figure 7. Snapshots of the FDTD simulation at 7.2, 8.7, 9.8 and 11.3 ms. The colour bar represents the amplitude of the displacement. The 4 mm rounded tumour is highlighted.

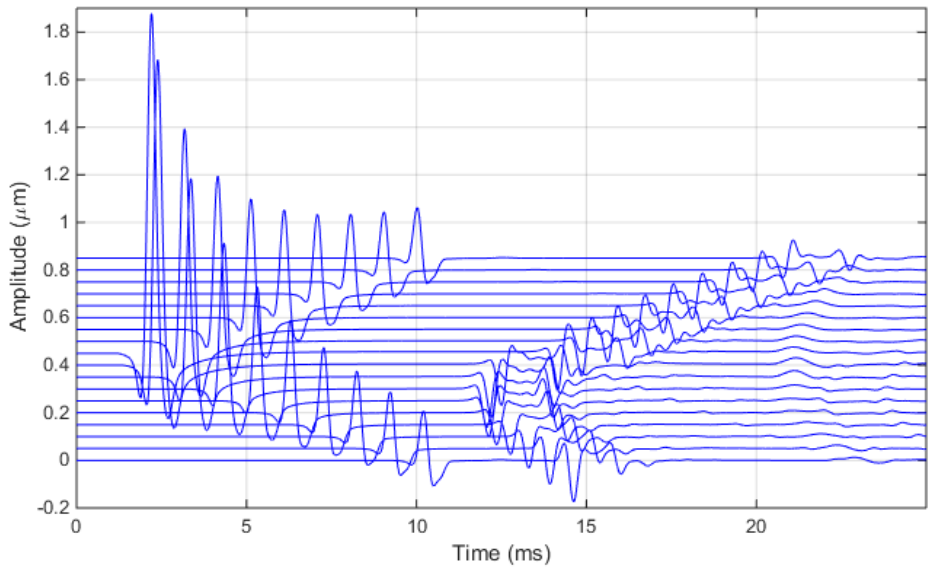

Figure 8. Recovered displacement signals at the 18 receivers. Distance between receivers 2.38 mm, with a 7.14 mm gap between receiver 9 and 10, where the excitation source is positioned.

Figure 9 depicts the reconstructed signal over the pseudo-experimental one. Recovered values for the tumour parameters and reconstruction errors are shown in Table 5. The errors were calculated over the search range established for each parameter. The algorithm showed good agreement between the reconstruction and the pseudo-experimental measurement.

Table 4. Discretization parameters for IP-AG testing

Variable	Description	Value
Δr	Radial dimension interval	150 µm
Δz	Depth dimension interval	150 µm
Δt	Time interval	17.32 µs
n_{PML}	Number of PML elements	40

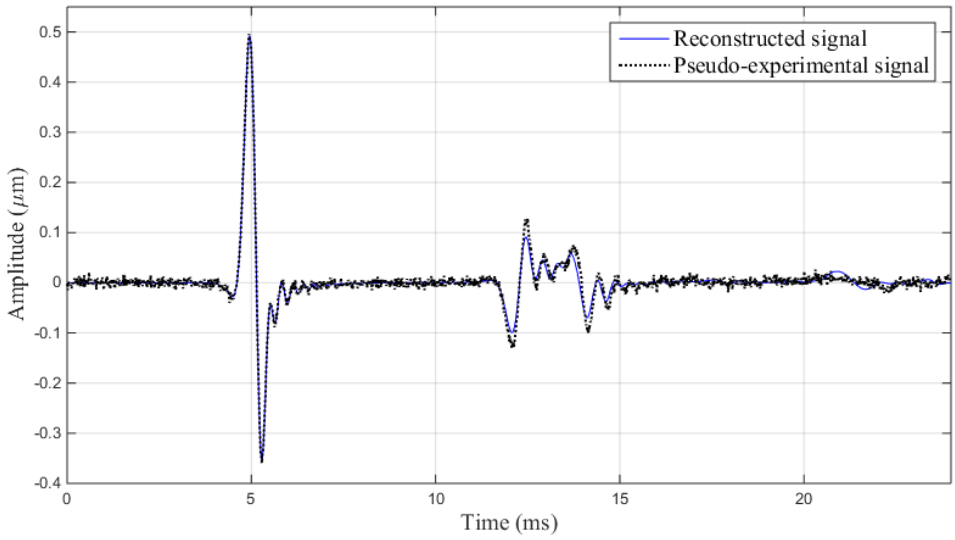

Figure 9. Reconstructed signal by using the IP-AG method (blue solid line) over the pseudo-experimental signal (black dotted line).

Table 5. Reconstructed values for the tumour parameters and reconstruction errors.

Parameter	Description	Original value	Reconstructed Value	Search Range	Error
r_c	Radial coordinate of the tumour	14.00 mm	13.7 mm	4 - 24 mm	3.10 %
z_c	Depth coordinate of the tumour	35.00 mm	36.98 mm	26 - 44 mm	3.96 %
$ø_c$	Diameter of the tumour	4.00 mm	3.63 mm	2 - 8 mm	6.16 %
μ_c	Shear modulus of cancerous tissue	18.00 kPa	16.61 kPa	16 - 21 kPa	9.56 %

4. Conclusion

A novel TU-SWE approach for diagnosis and ablation monitoring of PCa has been presented in this paper. It is based on the emission, detection and computational treatment of shear waves propagated into the prostate.

In order to study the feasibility of this approach, a FDTD model was developed to analyze the behavior of shear waves in a medium representative of prostatic tissue. Although the medium was assumed to be homogeneous and elastic, this was considered sufficient to simulate the mechanical behavior of the human prostate to a first approximation. The presence of cancerous nodules, which are usually stiffer than the surrounding healthy tissue, was also modelled. Reflections were generated when the wavefront hit the tumour, traveling back to the urethra where they were detected, demonstrating proof of principle and warranting further studies.

The IP-AG reconstruction method was tested by using the FDTD model for generating a pseudo-experimental signal and also as a forward model for searching the solutions within the IP algorithm. The results from the test showed good agreement between the pseudo-experimental signal and the reconstructed one, with an admissible level of error in the recovery of tumour parameters.

In further studies, a more realistic 3D model will be required, taking into account the heterogeneity and mechanical complexity of the human prostate. Experimental tests in prostate phantoms will be also required. In the IP ambit, it is of interest to study the probability of producing a false positive diagnosis, as well as how the response of the system changes with increasing levels of noise.

5. Acknowledgements

The authors would like thank P. Gelat for constructive and illuminating discussions. This research was supported by the Ministry of Education DPI2014-51870-R and DPI2010-17065, and Junta de Andalucía for projects P11-CTS-8089 and GGI3000IDIB. First author was supported by Talentia Scholarship C2012F1-75146405T-1, Agencia del Conocimiento Junta de Andalucía.

References

[1] Cancer Research UK 2014 Prostate cancer Key Stats *Cancer Res. UK*
[2] The Prostate Cancer Charity UK 2015 What is my risk of prostate cancer? *Prostate Cancer UK*
[3] Abdellaoui A, Iyengar S and Freeman S 2011 Imaging in prostate cancer *Futur. Oncol.* 679–91
[4] Kelloff G J, Choyke P and Coffey D S 2009 Challenges in clinical prostate cancer: role of imaging *AJR. Am. J. Roentgenol.* **192** 1455–70
[5] Lemaitre L, Puech P, Poncelet E, Bouyé S, Leroy X, Biserte J and Villers A 2009 Dynamic contrast-enhanced MRI of anterior prostate cancer: Morphometric assessment and correlation with radical prostatectomy findings *Eur. Radiol.* **19** 470–80
[6] Lim H K, Kim J K, Kim K a. and Cho K S 2009 Prostate cancer: Apparent diffusion coefficient map with T2-weighted images for detection - A multireader study *Radiology* **35** 100–100
[7] Langer D L, Van Der Kwast T H, Evans A J, Trachtenberg J, Wilson B C and Haider M a. 2009 Prostate cancer detection with multi-parametric MRI: Logistic regression analysis of quantitative T2, diffusion-weighted imaging, and dynamic contrast-enhanced MRI *J. Magn. Reson. Imaging* **30** 327–34
[8] Correas J M, Drakonakis E, Isidori a. M, Hélénon O, Pozza C, Cantisani V, Di Leo N, Maghella F, Rubini a., Drudi F M and D'ambrosio F 2013 Update on ultrasound elastography: Miscellanea. Prostate, testicle, musculo-skeletal *Eur. J. Radiol.* **82** 1904–12
[9] Tuxhorn J a, Ayala G E and Rowley D R 2001 Reactive stroma in prostate cancer progression. *J. Urol.* **166** 2472–83
[10] Tuxhorn J a, Ayala G E, Smith M J, Smith V C, Dang T D and Rowley D R 2002 Reactive Stroma in Human Prostate Cancer : Induction of Myofibroblast Phenotype and Extracellular Matrix Remodeling Reactive Stroma in Human Prostate Cancer : Induction of Myofibroblast Phenotype and Extracellular **8** 2912–23
[11] Burns-Cox N, Avery N C, Gingell J C and Bailey a J 2001 Changes in collagen metabolism in prostate cancer: a host response that may alter progression. *J. Urol.* **166** 1698–701
[12] Bamber J, Cosgrove D, Dietrich C F, Fromageau J, Bojunga J, Calliada F, Cantisani V, Correas J-M, D'Onofrio M, Drakonaki E E, Fink M, Friedrich-Rust M, Gilja O H, Havre R F, Jenssen C, Klauser a S, Ohlinger R, Săftoiu A, Schaefer F, Sporea I and Piscaglia F 2013 EFSUMB guidelines and recommendations on the clinical use of ultrasound elastography. Part 2: Clinical applications. *Ultraschall Med.* **34** 238–53
[13] Doherty J, Trahey G, Nightingale K and Palmeri M 2013 Acoustic radiation force elasticity imaging in diagnostic ultrasound *IEEE Trans. Ultrason. Ferroelectr. Freq. Control* **60** 685–701
[14] Ophir J, Alam S K, Garra B S, Kallel F, Konofagou E E, Krouskop T, Merrit C R B, Righetti R, Souchon R, Srinivasan S and Varghese T 2002 Elastography : Imaging the Elastic Properties

of Soft Tissues with Ultrasound *J. Med. Ultrason.* **29** 155–71
[15] Bercoff J, Tanter M and Fink M 2004 Supersonic Shear Imaging : A New Technique for Soft Tissue Elasticity Mapping **51** 396–409
[16] Barr R G, Memo R and Schaub C R 2012 Shear wave ultrasound elastography of the prostate: initial results *Ultrasound Q.* **28** 13–20
[17] Correas J M, Tissier A-M, Khairoune A, Vassiliu V, Méjean A, Hélénon O, Memo R and Barr R G 2015 Prostate Cancer : Diagnostic Performance of Real-time Shear-Wave Elastography *Radiology* **275** 280–9
[18] Ahmad S, Cao R, Varghese T, Bidaut L and Nabi G 2013 Transrectal quantitative shear wave elastography in the detection and characterisation of prostate cancer *Surg. Endosc.* **27** 3280–7
[19] Woo S, Kim S Y, Lee M S, Cho J Y and Kim S H 2015 Shear wave elastography assessment in the prostate: an intraobserver reproducibility study *Clin. Imaging* **39** 484–7
[20] Boehm K, Salomon G, Beyer B, Schiffmann J, Simonis K, Graefen M and Budaeus L 2015 Shear Wave Elastography for Localization of Prostate Cancer Lesions and Assessment of Elasticity Thresholds: Implications for Targeted Biopsies and Active Surveillance Protocols *J. Urol.* **193** 794–800
[21] Chopra R, Arani A, Huang Y, Musquera M, Wachsmuth J, Bronskill M and Plewes D 2009 In vivo MR elastography of the prostate gland using a transurethral actuator. *Magn. Reson. Med.* **62** 665–71
[22] Arani A, Plewes D and Chopra R 2011 Transurethral prostate magnetic resonance elastography: prospective imaging requirements. *Magn. Reson. Med.* **65** 340–9
[23] Arnal B, Pernot M and Tanter M 2011 Monitoring of thermal therapy based on shear modulus changes: I. Shear wave thermometry *IEEE Trans. Ultrason. Ferroelectr. Freq. Control* **58** 369–78
[24] Arnal B, Pernot M and Tanter M 2011 Monitoring of thermal therapy based on shear modulus changes: II. Shear wave imaging of thermal lesions *IEEE Trans. Ultrason. Ferroelectr. Freq. Control* **58** 1603–11
[25] Cohen R J, Shannon B a., Phillips M, Moorin R E, Wheeler T M and Garrett K L 2008 Central Zone Carcinoma of the Prostate Gland: A Distinct Tumor Type With Poor Prognostic Features *J. Urol.* **179** 1762–7
[26] Bohyun K and Chan K K 2013 Embryology, Anatomy and Congenital Anomalies of the Prostate and Seminal Vesicles *Abdominal Imagin* pp 1797–812
[27] Orescanin M, Member S and Wang Y 2011 3-D FDTD Simulation of Shear Waves for Evaluation of Complex Modulus Imaging *IEEE Trans. Ultrason. Ferroelectr. Freq. Control* **58** 389–98
[28] Jiménez N, Picó R, Camarena F, Redondo J and Roig B 2012 Ultrasonic evaluation of the hydration degree of the orange peel *Postharvest Biol. Technol.* **67** 130–7
[29] Virieux J 1986 P-SV wave propagation in heterogeneous media: Velocity-stress finite-difference method *Geophysics* **51** 889–901
[30] Leutenegger T and Dual J 2004 Non-destructive testing of tubes using a time reverse numerical simulation (TRNS) method *Ultrasonics* **41** 811–22
[31] Liu Q H 1999 Perfectly matched layers for elastic waves in cylindrical and spherical coordinates *J. Acoust. Soc. Am.* **105** 2075–84
[32] Gallego R and Rus G 2004 Identification of cracks and cavities using the topological sensitivity boundary integral equation *Comput. Mech.* **33** 154–63
[33] Rus G, Wooh S C and Gallego R 2007 Processing of ultrasonic array signals for characterizing defects. Part II: Experimental work *IEEE Trans. Ultrason. Ferroelectr. Freq. Control* **54** 2139–45